

Dynamics of Composite Domain Walls in Multiferroics in Magnetic Field and Their Instability

Koji Kawahara and Hirokazu Tsunetsugu

The Institute for Solid State Physics, The University of Tokyo, Kashiwanoha 5-1-5, Chiba 277-8581, Japan

We study theoretically the dynamics of composite domain walls (DW) in multiferroic material GdFeO_3 driven by magnetic field H . Two antiferromagnetic orders of Fe and Gd spins interact Gd-ion displacement in this system with coupling c at low temperatures, and we have numerically simulated the corresponding time-dependent Ginzburg-Landau equations in which magnetic field H couples to Fe-spin order parameter. We vary H and c systematically and calculate velocity v and inner structure in a stationary state for magnetic DW and magneto-electric DW. DW mobility v/H increases with H and decreases with c for both DWs, but their characteristics differ between the two. We have also studied analytically the smooth characteristics of magneto-electric DW by a perturbation theory. Another finding is a splitting instability at large H . A magneto-electric DW splits into a pair of magnetic DW and electric DW when c is large, while a magnetic DW splits when c is small. Internal structure of composite DW deforms with increasing c and H , and modulations in different order parameters separate in space. Their relative distances show a noticeable enhancement with approaching the splitting instability.

1. Introduction

Multiferroic materials are a system in which multiple macroscopic orders coexist, and a rich play ground of physics of both fundamental and application interests.¹⁻⁴⁾ They exhibit complex low-temperature ordered phases. Extensive researches have been performed for clarifying microscopic origin of multiferroic phases⁵⁾ and also symmetry conditions.⁶⁾ The multiferroic phases have domain walls (DWs) as a topological defect,⁷⁾ and their internal structure is affected by interactions between multiple order parameters. These DWs are often called *composite domain wall*,⁸⁾ when several order parameters “flip” around the same place. Low-temperature phases and their DW excitations have been experimentally studied in detail for several multiferroics such as TbMnO_3 ,⁹⁾ GdFeO_3 ,⁸⁾ and RMnO_3 .^{10,11)} As for application interests, multiferroics is a candidate of new low-energy consuming memory device using cross correlations.^{12,13)} For example, it is possible to flip or reorient magnetic moments by applying electric field. This effect originates in either reorientation of bulk spins,¹⁴⁾ or creeping motion of composite DW.¹⁵⁾

An important issue is how the interaction between different orders affects the dynamics of the system. Multiple orders in multiferroic materials have their intrinsic time and length scales that differ from each other. When their interaction takes effect, the dynamics of the coupled system becomes non-trivial, and it is important to understand their characteristics. The DW dynamics in a system with single order parameter is quite well understood. Bloch DW in uniaxial magnet is driven by magnetic field and its dynamics is described by Walker’s solution,¹⁶⁾ which predicts a linear velocity-field characteristic. A recent study also discussed a turbulent DW motion at high field.¹⁷⁾ It is also known that electric current drives magnetic DW by spin transfer effect.^{18,19)} For multifer-

roics, there are several studies on their bulk dynamics as well as static DW. Optical responses were studied based on a spin model¹⁴⁾ and also first principal calculation.²⁰⁾ Spin reorientation process of bulk spin under magnetic field was experimentally visualized and analyzed by micromagnetic simulation of Landau-Lifshitz-Gilbert equation.²¹⁾ Spatial structure of static composite DWs was studied using a Ginzburg-Landau model for magneto-electric multiferroic materials such as BiFeO_3 ,²²⁾ and also ferroelectric-ferroelastic DW in BiFeO_3 .²³⁾ The former case has two order parameters. The latter case has three order parameters, and instability of static DW was examined. Several interesting phenomena are found such as enhancement of order parameter around DW²²⁾ and transverse deformation of DW.²³⁾

In this paper, we will investigate dynamics of composite DW, and the main target material is GdFeO_3 . In this system, three order parameters interact at low temperatures, and they are two antiferromagnetic orders and lattice distortion. One antiferromagnetic order is made of Fe spins and staggered Dzyaloshinsky-Moriya interactions^{24,25)} generate parasitic weak ferromagnetic moments. Ferroelectricity originates in displacement of Gd ions induced by interactions with antiferromagnetic orders of Fe and Gd spins, and this appears at $T < 4\text{K}$. Thus, this is one of the typical multiferroic materials with both ferromagnetism and ferroelectricity.^{8,27)} Composite DWs differ in one important point from DWs in the systems with single order parameter, and that is multiple types of composite DWs depending on which order parameters change. Since the low-temperature phase of GdFeO_3 has three types of order parameters, there are three types of composite DWs.⁸⁾

The main issue to study in this work is how the coupling c between the three order parameters changes the internal structure and dynamics of composite DWs. A fundamental

question is how the coupling changes velocity of DW driven by magnetic field H . By simulating phenomenological time-evolution equations, we study this dynamics and calculate the DW velocity in the stationary state with varying field H and coupling c . We will show that increasing H not only accelerates the velocity of composite DWs but also destabilizes them. It is interesting that this instability depends on their DW type as will be shown later. We also perform an analytical calculation for correction in DW velocity due to the coupling, when c and H are both small. This DW instability is also related to another question about the inner structure of composite DWs. We will calculate spatial profile of the multiple order parameters inside a DW, and find that it also demonstrates a precursor of the DW instability. For simplicity, we limit our study in this work to the case that order parameters vary only along one direction of space. Therefore, transverse thermal fluctuations inside DW region are neglected, which may be justified at low temperatures.

This paper is organized as follows. In Sec. 2, we explain our phenomenological model including the interaction c among multiple order parameters, basics of composite DWs, and time-evolution equations to solve. In Sec. 3, we numerically solve these equations for DWs driven by magnetic field H and calculate their velocity v . The scaling of $v(c, H)$ is analyzed in detail. In Sec. 4, we investigate an instability of DWs based on numerical results, and analyze internal structure of DWs. In Sec. 5, we formulate a perturbative theory when the interaction c is small. The last section is conclusions.

2. Model

In this paper, we study the dynamics of composite DW in the typical multiferroic material GdFeO_3 . This has a crystal structure that contains two magnetic sublattices comprised of Fe and Gd ions each, and exhibits both complex magnetic order and ferroelectricity at low temperatures below 4 [K]. At temperatures $T < 650$ [K], Fe spins show an antiferromagnetic order accompanied by weak ferromagnetic order. Below the transition at 4 [K], Gd spins show an antiferromagnetic order, and ferroelectricity appear at the same time.^{8,28)} The crystal and magnetic structures are shown in Fig. 1. Magnetic structure of Fe and Gd spins is the type $G_xA_yF_z$ and G_xA_y , respectively, in Bertaut notation,²⁹⁾ and thus the z -component of Fe spins is weak ferromagnetic moment. Ferroelectricity is induced by antiferromagnetic interactions between Fe and Gd spins via "exchange-striction mechanism", which leads to uniform displacement of Gd ions.⁸⁾ Interactions between each spins are also estimated both experimentally³⁰⁾ and by first principle calculation.²⁰⁾

2.1 Ginzburg-Landau free energy

We employ a coarse-grained model instead of microscopic spin Hamiltonian to study the dynamics of composite DW, since it is more convenient to study a large-size object. That is the Ginzburg-Landau free energy model for GdFeO_3 and it is represented in terms of three continuous field variables: local antiferromagnetic moments of Fe and Gd spins $N(\mathbf{r})$ and

$\mathbf{n}(\mathbf{r})$ and ferroelectric polarization density $P(\mathbf{r})$

$$F = F[N(\mathbf{r}), \mathbf{n}(\mathbf{r}), P(\mathbf{r})] = \int d\mathbf{r} \mathcal{F}(\mathbf{r}), \quad (1a)$$

$$\mathcal{F} = \mathcal{F}_0 + \mathcal{F}_1, \quad \mathcal{F}_0 = \mathcal{F}_F + \mathcal{F}_G + \mathcal{F}_P, \quad (1b)$$

where each part of the order parameters reads

$$\mathcal{F}_F = \frac{\kappa}{2}(\nabla N)^2 - \frac{a}{2}|N|^2 + \frac{b}{4}|N|^4 + \sum_{\nu=x,y,z} \frac{\alpha_\nu}{2}(N_\nu)^2 - HN_x, \quad (2a)$$

$$\mathcal{F}_G = \frac{\kappa'}{2}(\nabla \mathbf{n})^2 - \frac{a'}{2}|\mathbf{n}|^2 + \frac{b'}{4}|\mathbf{n}|^4, \quad (2b)$$

$$\mathcal{F}_P = \frac{K}{2}(\nabla P)^2 + \frac{A}{2}P^2. \quad (2c)$$

The interaction part \mathcal{F}_1 will be explained later. Both of N and \mathbf{n} are 3-component vector fields, and we will sometimes use the polar representation

$$\begin{aligned} N &= |N|(\sin \theta_F \cos \phi, \sin \theta_F \sin \phi, \cos \theta_F), \\ \mathbf{n} &= |\mathbf{n}|(\sin \theta_G \cos \psi, \sin \theta_G \sin \psi, \cos \theta_G). \end{aligned} \quad (3)$$

Electric polarization P originates in the z -component of Gd ion displacement. α_ν 's are onsite biaxial anisotropy constants of Fe spins (x -easy, z -hard); $\alpha_x < \alpha_y < \alpha_z = 0$, while Gd spins are isotropic.¹⁵⁾

Magnetic field H couples to the x -component of staggered moment of Fe spins. Of course, this is not a direct Zeeman coupling but an effective one. The staggered component of Fe-spin moments couples to the uniform component through staggered Dzyaloshinsky-Moriya interactions.^{8,24,25)} Since uniform magnetic field \mathbf{h} induces the uniform component, the coupling has a form $-(\mathbf{D}^{\text{stag}} \times \chi \mathbf{h}) \cdot \mathbf{N}$ where χ is the magnetic susceptibility tensor. When \mathbf{h} is applied along z -axis and y -component is active in \mathbf{D}^{stag} , this form is reduced to $-HN_x$ with $H = D_y^{\text{stag}} \chi_{zz} h_z$. In our model, we use the induced effective staggered field H , instead of bare uniform field h_z for simplicity.

The interaction has a multi-linear form of the three order parameters⁸⁾

$$\mathcal{F}_1 = cPN \cdot \mathbf{n}. \quad (4)$$

One can show this form of coupling based on symmetry argument, but we will examine a condition of $c \neq 0$ starting from a microscopic model. The starting model is a Heisenberg model in which the antiferromagnetic coupling $J_{FG}(R_{12})$ between nearest-neighbor Gd and Fe spins varies with their distance R_{12} . This implies that J_{FG} modulates in space with the displacement vector $\mathbf{D}(\mathbf{r})$ of Gd ions. Assuming the isotropic proportionality $\mathbf{P}(\mathbf{r}) = \zeta \mathbf{D}(\mathbf{r})$, the result of leading-order coupling is written as

$$c = g_{12} \zeta^{-3} \langle P_x(\mathbf{R})P_y(\mathbf{R}) \rangle_{\text{av}}, \quad (5)$$

where the average is taken over all the Gd sites \mathbf{R} . The pref-

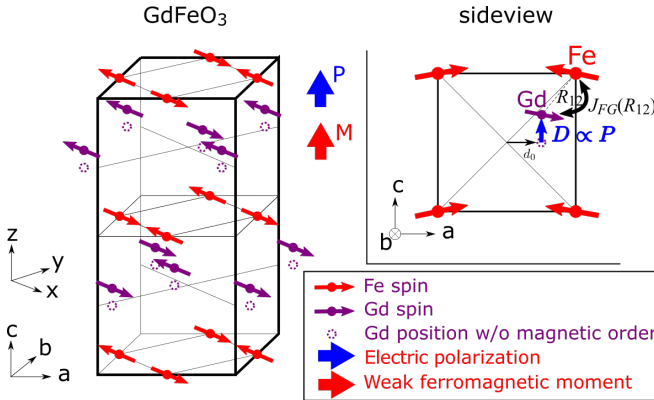


Fig. 1. Magnetic unit cell of GdFeO_3 with no external field below 4 [K]. a , b , and c denote crystallographic axes, while x , y , and z are quasi-cubic axes.

actor is given by

$$g_{12} = R^{-3} \bar{\nabla}(\bar{\nabla} - 2)(\bar{\nabla} - 4)J_{FG}(R) \Big|_{R=\bar{R}_{12}}, \quad (6)$$

where \bar{R}_{12} is the average nearest-neighbor distance between Fe and Gd sites and the dimensionless derivative is defined as $\bar{\nabla} = d/d \log R$. Therefore, Fe and Gd antiferromagnetic moments couple to each other mediated by a ferro quadrupole of Gd-ion displacements. This quadrupole has a nonzero amplitude when Gd-ion displacements have a staggered order in their x and y components. This is the case of GdFeO_3 , but the above condition is satisfied by many other situations. One example is the case that each of x and y component is random in space but their product has a uniform order, which is an intrinsic quadrupole order of displacements.

2.2 Bulk states and composite domain walls

Stable bulk state is the uniform state with free energy F minimum. Since it is a vacuum of topological defects such as DWs, it is important to determine it first. When no magnetic field is applied $H = 0$, stable bulk state has 4-fold degeneracy

$$N_{\text{eq}}(\mathbf{r}) = N_{\text{eq}} = \pm(N_0, 0, 0), \quad (7a)$$

$$\mathbf{n}_{\text{eq}}(\mathbf{r}) = \mathbf{n}_{\text{eq}} = \pm(n_0, 0, 0), \quad (7b)$$

$$P_{\text{eq}}(\mathbf{r}) = P_{\text{eq}} = -\frac{c}{A}N_{\text{eq}} \cdot \mathbf{n}_{\text{eq}} = \pm\frac{c}{A}N_0n_0, \quad (7c)$$

where

$$\begin{bmatrix} N_0^2 \\ n_0^2 \end{bmatrix} = \frac{1}{bb' - c^4/A^2} \begin{bmatrix} b' & c^2/A \\ c^2/A & b \end{bmatrix} \begin{bmatrix} a - \alpha_x \\ a' \end{bmatrix}. \quad (7d)$$

Note that the sign of P_{eq} is determined from $N_{\text{eq}} \cdot \mathbf{n}_{\text{eq}}$. Both \mathbf{N} and \mathbf{n} point to x -axis, the easy axis of Fe spins. These four stable states are shown in Fig. 2.

DWs have a finite excitation value of free energy and connect different stable states. In GdFeO_3 , two of the three order parameters continuously flip in DW as pointed out by Toku-naga et al.⁸⁾ Flipping one order parameter is energetically prohibited, because it costs not local but bulk energy of the inter-

action term \mathcal{F}_1 . Depending on which two are flipped, DWs are categorized into three types shown in Fig. 2.

The first type is magnetic domain wall (M-DW), in which \mathbf{N} and \mathbf{n} flip and correspondingly the weak ferromagnetic moment also flips. The second type is electric domain wall (E-DW), in which \mathbf{n} and electric polarization P flip. The third type is magneto-electric domain walls (ME-DW), in which \mathbf{N} and P flip. This time the weak ferromagnetic moment M and electric polarization P flip simultaneously. In each of these three types, at least one antiferromagnetic order parameter rotate inside a DW during its flipping process. The spin anisotropy confines this rotation in the xy -plane, and this rotation defines its chirality ± 1 corresponding to clockwise and anticlockwise rotation. Therefore, there are 6 types of DW in total.

2.3 Time-dependent Ginzburg-Landau equations

We will analyze the dynamics of DWs in the following sections, and need to choose equations of motion of the order parameters. Since none of the order parameters are conserved quantities, we use in this work the time-dependent Ginzburg-Landau (TDGL) equation.³²⁾ An alternative approach¹³⁾ used a Lagrangian formulation for collective coordinates of DW and studied precession of sublattice magnetizations. In this paper, we focus on dissipation-driven effects on DW dynamics and use the TDGL formulation. Namely, the velocity of order parameters follows the force generated by local free energy. The general TDGL formulation implies $\partial_t \mathcal{O}(\mathbf{r}, t) = -\gamma_{\mathcal{O}} \delta F / \delta \mathcal{O}(\mathbf{r}, t)$ for each order parameter field $\mathcal{O} = \mathbf{N}$, \mathbf{n} , or P . The right-hand side is a functional derivative of the total free energy (1a) defined by the order parameters at time t . Note that we do not include white noises, which are sometimes added to the deterministic forces. In the present case, the TDGL equations read

$$\begin{aligned} \gamma^{-1} \partial_t N_{\nu}(\mathbf{r}, t) &= (\kappa \nabla^2 + a - \alpha_{\nu} - b N^2) N_{\nu} \\ &+ H \delta_{\nu, x} - c P n_{\nu}, \end{aligned} \quad (8a)$$

$$\gamma'^{-1} \partial_t n_{\nu}(\mathbf{r}, t) = (\kappa' \nabla^2 + a' - b' \mathbf{n}^2) n_{\nu} - c P N_{\nu}, \quad (8b)$$

$$\Gamma^{-1} \partial_t P(\mathbf{r}, t) = (K \nabla^2 - A) P - c \mathbf{N} \cdot \mathbf{n}, \quad (8c)$$

for $\nu = x, y$, and z , and $\delta_{\nu, x}$ is Kronecker delta. The coefficients γ , γ' , and Γ are phenomenological relaxation constants. In the next sections, we will perform both numerical and analytical analyses of this set of TDGL equations.

Before analyzing the dynamics of composite DWs, let us recall the result of a simple case of no interaction $c = 0$ and flat DW, *i.e.*, one-dimensional \mathbf{r} -dependence. In this case, external field H drives only Fe order parameter N . When the amplitude modulation is small, its stationary state solution is

$$\mathbf{N}(\mathbf{r}, t) = N_0(\cos \phi_s(\xi), \sin \phi_s(\xi), 0), \quad (9a)$$

$$\xi = x - \mu_0 H t + x_0, \quad \mu_0 \equiv \gamma N_0 \sqrt{\frac{\kappa}{\alpha_y - \alpha_x}}. \quad (9b)$$

The functional form of ϕ_s will be given later in Eq. (23) and

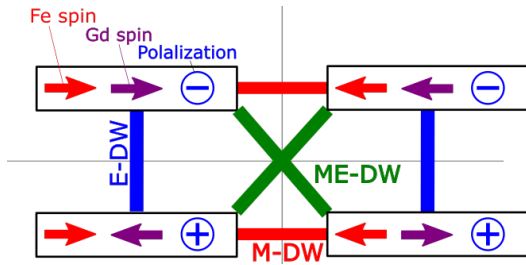


Fig. 2. Four degenerate stable states in the model. Arrows represent spins along easy axis (x -axis), and electric polarization is represented by the sign of its z -component. Lines connecting different stable states correspond to three types of domain walls; electric (E-DW), magneto-electronic (EM-DW), and magnetic (M-DW).

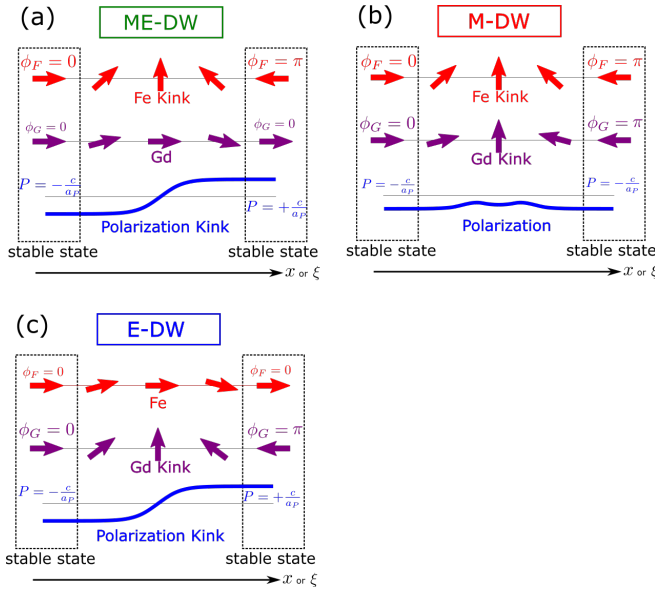


Fig. 3. Schematics of inner structures of (a) multiferroic (b) magnetic (c) electric DWs driven by magnetic H or electric E field. Arrows show spin directions versus the boosted coordinate ξ moving with domain wall. In each DW, two out of the three order parameters flip, while the non-flipping order parameter is modulated around the DW center.

x_0 is a constant determined by the initial condition. Therefore, the terminal velocity of DW motion is linear in the applied field H

$$v = \mu_0 H. \quad (10)$$

This means that the coefficient μ_0 is a DW mobility at $c = 0$ and it is proportional to the DW width $\ell_0 = N_0 \sqrt{\kappa} / (\alpha_y - \alpha_x)$. Further details will be explained in Sec. 5. It is important that the $v-H$ relation has no higher-order corrections, because the DW at $c = 0$ has only one length scale ℓ_0 .

In the following sections, we will study DW dynamics driven by an external field H . We will calculate DW velocity in a stationary state and analyze how it depends on the coupling c of multiple orders. We will also study how the internal structure in DW deforms in moving DW.

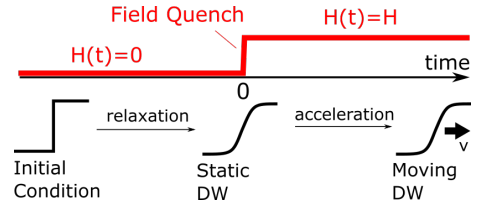


Fig. 4. Simulation protocol and schedule of field control.

Table I. Model parameters in TDGL simulation

relaxation constants	$\gamma = \gamma' = \Gamma = 1.0$
stiffness	$(\kappa, \kappa', K) = (20, 4, 0.04)$
anisotropy	$\alpha = (-0.5, -0.2, 0)$
Fe bulk term	$(a, b) = (100, 100)$
Gd bulk term	$(a', b') = (100, 100)$
P bulk term	$A = 0.11$

3. Numerical analysis of DW velocity

In this section, we use numerical simulation and study the dynamics of composite DWs driven by magnetic field H . To this end, we numerically integrate the TDGL equations (8a)-(8c) with the protocol shown in Fig. 4 and calculate the velocity. Since the one-dimensional DW structure is concerned, the Laplacian is replaced as $\nabla^2 \rightarrow \partial_x^2$. In the first part of the protocol, no field is applied and we integrate the equations Eqs. (8a)-(8c) to obtain a stable static DW solution. This has a DW in two of the order parameters in zero magnetic field. In the second part, we apply a nonzero field H and numerically track the time evolution of the order parameter fields until the DW velocity converges to a constant value. Note that $v(c, H)$ has natural symmetry $v(c, -H) = -v(c, H)$ as will be shown explicitly for the simplified model in Sec. 5. Our choice for an initial state in the first part is the configuration that left and right parts are different stable bulk states among the four defined in Eqs. (7a)-(7c). Chirality of DW, direction of spin rotation in xy -plane, is set in the initial condition. We have calculated velocity of two types of composite DWs. One is ME-DW and N_x and P change their sign. The other is M-DW and N_x and n_x change sign. Note that P-DW does not couple to magnetic field.

Let us summarize parameters used in the numerical simulations. The range $-100 \leq x \leq 100$ is used for the entire space and discretized to 500 grid points. The system size is thus $L = 200$. Open boundary condition is used. As a DW moves, we follow its motion and shift the simulation region. The coupling constants in the free energy (1b) are set to the values listed in Table I. Here, the identical value is set to all the relaxation constants for simplicity. Anisotropy parameter α is set to describe experimental observation of magnetic moments. For stiffness constant, K for polarization P is set smaller than those for N and n , since DW in ferroelectrics is generally much narrower than in magnets. In magnets it is typically the order of $\sim 100\text{\AA}$,²⁾ much larger than in BaTiO_3 ,³⁴⁾ a ferroelec-

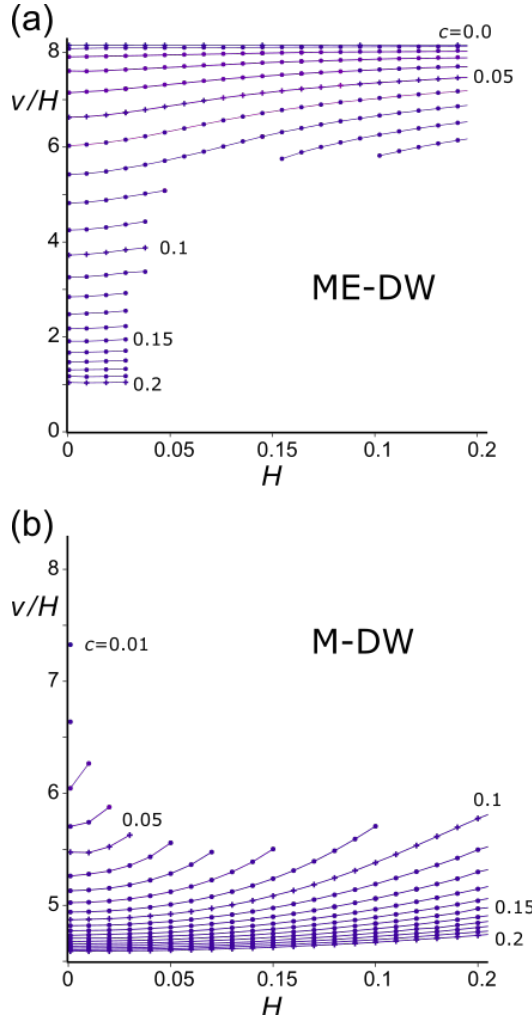


Fig. 5. Domain wall velocity normalized by H versus H . (a) ME-DW and (b) M-DW. The interaction c changes in the range $0 \leq c \leq 0.2$ by 0.01, but (b) has no data for $c = 0$. Minimum H tested is $H = 0.001$. Note that the vertical axis has a different scale in (a) and (b).

tric compound with the same structure with GdFeO_3 .

For numerical integration, we have used the fourth- and fifth-order Runge-Kutta-Fehrberg method.³¹⁾ We have used an adaptive discretization method for time so that the difference between the fourth and fifth order calculations is small enough for each order parameter. Typical time step is the order of $\Delta t \sim 0.01$.

When the coupling is $c = 0$, the amplitude of Fe moment is $N_0 = \sqrt{(100 + 0.5)/100} = 1.0025$. The mobility of its DW is calculated from Eq. (9b)

$$\mu_0 = 1.0025 \cdot \sqrt{20/0.3} = 8.185. \quad (11)$$

For $c > 0$, following the above procedures, we have calculated the terminal velocity $v(c, H)$ in the stationary state for ME-DW and M-DW with varying both magnetic field H and the coupling c . Figure 5 shows the plots of $v(c, H)/H$ versus H for $0 \leq c \leq 0.2$. The ratio v/H is an effective DW mo-

bility. Data are missing at some H -values when c is large for ME-DW and small for M-DW. This is related to the instability of these composite DWs and we will discuss this issue in the next section.

The main characteristics of the effective mobility $v(c, H)/H$ are as follows. First, this is a monotonic function in both H and c but with opposite trends. The DW velocity and thus mobility slow down as the coupling c increases. This agrees with an intuitive expectation that c enhances dissipation, because it induces dragging the fields \mathbf{n} and P , which do not directly couple to H . Concerning the H -dependence, the effective mobility grows monotonically with H . It is important that it however never exceeds the value at $c = 0$

$$v(c, H)/H \leq \mu_0, \quad (12)$$

for all the values of c and H examined. Secondly, ME-DW and M-DW have different characteristics, particularly about c dependence of velocity. We have continued calculation up to the largest value of $c = 0.5$, and found that the effective mobility at $H \sim 0$ goes down to a small value ~ 0.10 for ME-DW. The scaling in the large- c region is

$$v(c, H)/H|_{H \sim 0} \sim 0.044c^{-2}, \quad (0.2 \leq c \leq 0.5). \quad (13)$$

In contrast to this, the mobility of M-DW remains a much larger value ~ 4.5 and shows a saturating behavior. It is noticeable that M-DW becomes unstable with $c \rightarrow 0$, but ME-DW is stable in that region and has a large mobility. The H -dependence in the small- c region also differ in amplitude and more importantly in c -dependence.

Let us discuss the origin of these differences between these two DWs. One important difference is in the continuity when switching on the interaction c . At small c , the ME-DW solution has small $|P(x)| \propto c^1$ near both ends of the system. This continuously evolves from the solution $P(x) = 0$ at $c = 0$. As for the M-DW solution, $n_x(x)$ is nearly $+n_0$ at one end of the system but $-n_0$ at the other end. This implies that the initial value at $c = 0$ should be chosen as

$$\mathbf{n}(x) = \pm n_0 (\sin \pi x/L, \pm \cos \pi x/L, 0). \quad (14)$$

Here, L is the system size and very large (200 in our setting). This large length scale appears because the angular part of Gd spins has a critical Gaussian form of the bulk free energy. As the system has no intrinsic length scale, the system size determines the spatial variation of $\mathbf{n}(x)$. When switching on the interaction c , the \mathbf{n} field starts to couple to N and imports its length scale $\ell_0 \sim 8$. Therefore, the competition between the energy gain in the interaction part F_1 and the cost in the elastic energy of \mathbf{n} field is serious, and the evolution of M-DW with c is not as continuous as that of ME-DW. This yields qualitative different features in the c -dependence of $v(c, H)$ between the two types of composite DWs. We continue to analyze different features in more detail.

For analyzing H -dependence more quantitatively, let us expand the velocity in H as

$$v(c, H) = \alpha(c)H + \beta(c)H^3 + \dots \quad (15)$$

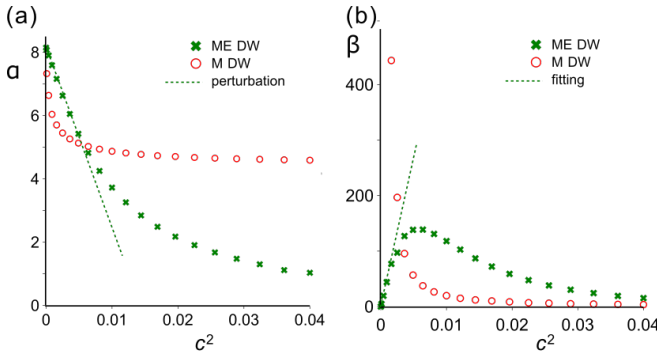


Fig. 6. Linear and the third-order coefficients of DW velocity in driving field $v(c, H) = \alpha(c)H + \beta(c)H^3 + \dots$

The symmetry when H is reversed ensures the relation $v(c, -H) = -v(c, H)$, as will be shown in Eq. (22) for a simplified model. Therefore, even-order terms vanish in the expansion. By fitting the data in Fig. 5, we have determined $\alpha(c)$ and $\beta(c)$ and plot the results versus c^2 in Fig. 6. $\alpha(c)$ and $\beta(c)$ are determined by fitting $v(c, H)$ in the range $H \leq 0.10$. Note that data of M-DW for $c \leq 0.04$ are missing, since the number of available data does not suffice due to DW instability. The linear coefficient α decreases monotonically with c for both DWs, but it remains quite a large value ~ 4.5 for M-DW. These features are consistent with the trends in Fig. 5 explained before. In the small- c region, the coefficient $\alpha(c)$ is well represented for ME-DW by

$$\alpha(c) = \mu_0 + v_{21}c^2 + O(c^4), \quad v_{21} = -601.3. \quad (16)$$

The coefficient $\alpha(c)$ for M-DW also decreases with c but c dependence is more complicated. It shows a very quick decrease for small c but then the decrease is strongly suppressed for $c > 0.01$.

The difference is more prominent in the third-order coefficient $\beta(c)$. For ME-DW, it starts from 0 and shows a linear increase in c^2 . The peak locates around $c = 0.07$ and after that $\beta(c)$ decreases smoothly. The c -dependence is completely different for M-DW, and $\beta(c)$ shows a divergent behavior as c approaches 0.

In summary, it is a general characteristics that the DW mobility increases with H and decreases with c , and this holds for both ME-DW and M-DW. However, analyticity of c -dependence differs between the two DWs. For ME-DW, the c -dependence is very smooth and can be represented by a power series. For M-DW, the c -dependence is continuous but cannot be represented by a simple power series in contrast to the case of ME-DW. This difference is attributed to a “singular” continuity of \mathbf{n} field in M-DW upon switching on the interaction c .

4. Splitting instability of DW

In this section, we discuss instability of composite DWs based on numerical results of their inner structure. We will show that the instability is a splitting into two composite DWs

of different types. This splitting is unique in that the presence of multiple orders determines how it splits. The possibility of a similar splitting was pointed out in Tokunaga’s work⁸⁾ as impurity effects around a pinning center. Our simulation has shown that splitting occurs in pure systems with no pinning centers. This means that the intrinsic inner structure of DW deforms and this leads a DW instability.

To study the origin of DW instability, we follow the time evolution of the order parameter fields $\mathbf{N}(x, t)$, $\mathbf{n}(x, t)$, $P(x, t)$ and see what happens when a composite DW is unstable. Figures 7 and 8 show a few snap shots of the field configurations for ME-DW and M-DW, respectively. (ϕ, θ_F) and (ψ, θ_G) are a set of polar and azimuthal angles of Fe and Gd spins, respectively in Eq. (3). Polarization P is plotted in the unit of $P_0 = |N_0 n_0 c/A|$. Length of spins $|N|$ and $|\mathbf{n}|$ stays close to equilibrium value N_0 and n_0 in Eq. (7), except a small drop typically $\sim 0.6\%$ around DW center. Let us see the ME-DW case first. At a time short after the field quench ($t = 0.89$), both \mathbf{N} and P fields have a nearly perfect DW and \mathbf{n} field is slightly modulated around their center. As time goes ($t = 23$ and 234), the two DWs are deformed and the DW in P field delays. This delay is natural, since magnetic field drives \mathbf{N} field and the drive to P field is indirect through the coupling c . At the same time, the modulation in \mathbf{n} is strongly enhanced around the DW in P field and eventually comes close to $\mathbf{n} \sim (-1, 0, 0)$ around $x = 90$ at $t = 234$. In this x -region, $\mathbf{N} \sim (-1, 0, 0)$ and $P \sim 1$, and this set together with $\mathbf{n} \sim (-1, 0, 0)$ corresponds to one of the four stable bulk states (7a)-(7c). Once this stable region appears, its size expands with time as shown by the data at $t = 445$. At the right end of this region, \mathbf{N} and \mathbf{n} flip constituting a M-DW and this moves to right. At the left end, \mathbf{n} and P flip constituting an E-DW and this stays at the position where it is created. Thus, one ME-DW is split into a pair of moving M-DW and unmoving E-DW. A similar process occurs for M-DW in Fig. 8. The DW in \mathbf{n} field delays and P modulation is enhanced around its center at the same time eventually to $P \sim 1$ around $x = 30$. Then, this creates a E-DW and the right end of the expanding new stable region becomes a ME-DW. Thus, in this case one M-DW is split into a pair of moving ME-DW and unmoving E-DW.

To examine c -dependence more systematically, we have calculated the deformation of DW inner structure with varying c . Define a characteristic position x_c for each order parameter field in a DW and plot their relative distances in the stationary state in Fig. 9 for $c = 0.04$ and 0.09 . For each order parameter that flips across a domain wall, x_c is defined by a point where its value is $\pi/2$ for ϕ and ψ and 0 for P . For a non-flipping order parameter, x_c is defined by a point of maximal deviation from the value at $x = \pm\infty$.

One can see two characteristic features in Fig. 9 with approaching the DW instability. First, the distances between $x_c(\text{Fe})$ and other two increase. However, the largest value just before instability depends on the value of c , and one cannot define a *universal* critical value of the relative distances. Secondly, the two distances become closer with approaching the instability. This is due to two contributions. One is that profile

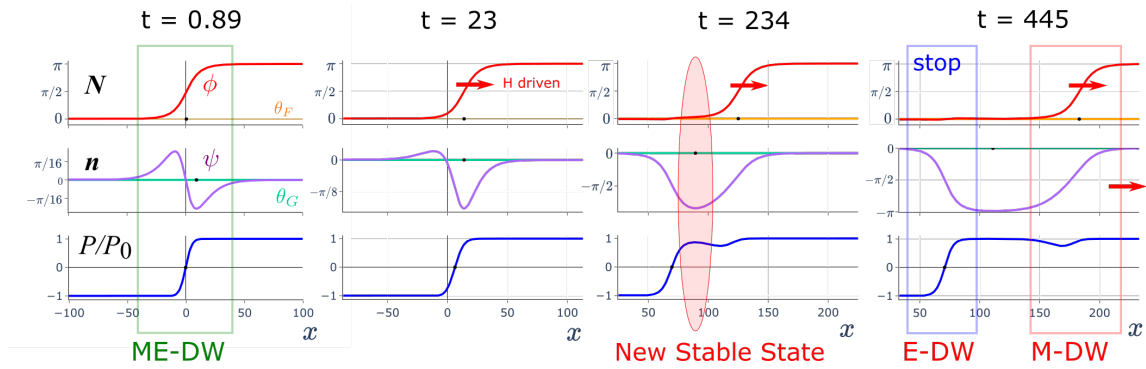


Fig. 7. Splitting of ME-DW into a pair of E-DW and M-DW. The panel for $t = 0.89$ shows stable static profiles. $c = 0.04$ and $H = 0.10$.

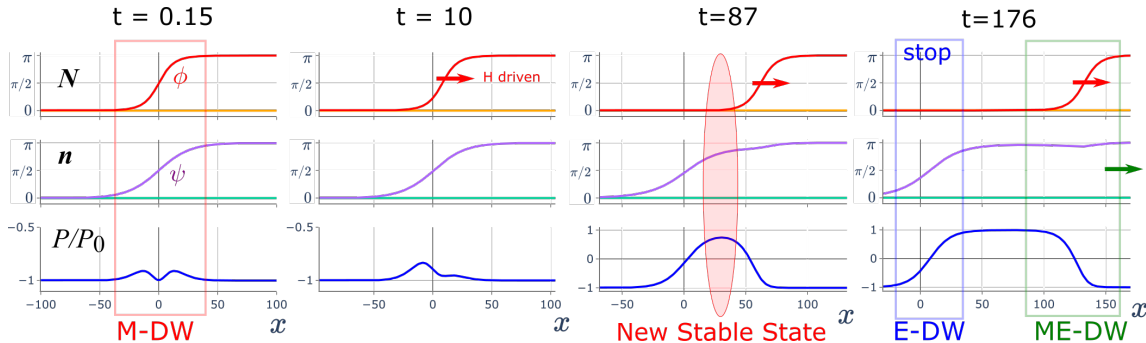


Fig. 8. Splitting of M-DW into a pair of E-DW and ME-DW. The panel for $t = 0.15$ shows stable static profiles. $c = 0.09$ and $H = 0.10$.

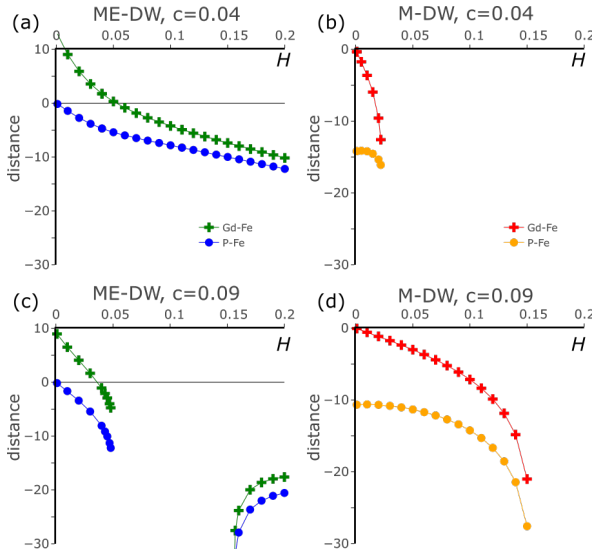


Fig. 9. Deformation of DW inner structure.

of non-flipping order parameters changes from a dispersive form to a single peak. The other is that the modulations in \mathbf{n} and P fields become more strongly coupled. It is interesting that the modulations in \mathbf{n} and P fields separate from $x_c(\text{Fe})$ by a distance a few times of ℓ_0 .

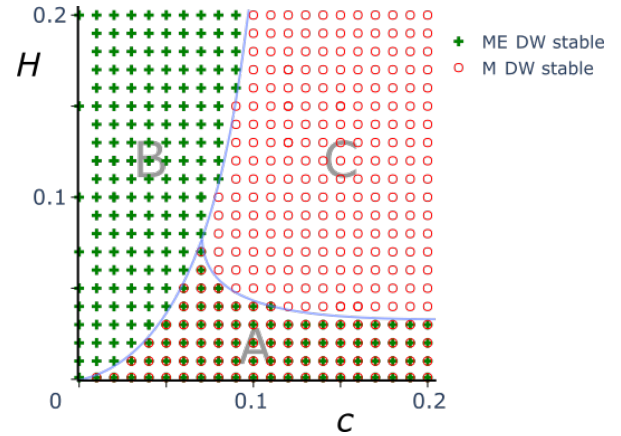


Fig. 10. Phase diagram of DW stability. Green crosses and orange dots show the points where ME-DW and M-DW is stable, respectively.

Figure 10 shows the non-equilibrium phase diagram of moving composite DWs in the (c, H) parameter space. In region B, M-DW is unstable and splits into a pair of moving ME-DW and nonmoving E-DW, while ME-DW is stable. In region C, ME-DW is unstable and splits into a pair of moving M-DW and nonmoving E-DW, while M-DW is stable. Therefore, regions B and C are dual to each other. In region A, ME-DW or M-DW are both stable and this is only the region

where one can drive both types of DWs without their splitting in applying magnetic field. One should note that its width is very small at small c but reasonably wide for $c \geq 0.7$. An interesting feature is a reentrant region $0.7 \leq c \leq 1.0$. In this region, increasing H first destabilizes a ME-DW, and it splits to a pair of M-DW and P-DW. However, increasing H further beyond a second critical value now destabilizes a generated M-DW and a ME-DW comes back. Boundary of phase B is approximated as $H_c \propto c^k$ with $k = 1.8 \pm 0.1$ for the part with region A, and $k = 3.0 \pm 0.1$ for the part with C.

This splitting instability is a result of deformation of DW inner structure, especially that of non-flipping order parameter. For ME-DW, increasing c and H enhances deformation in ψ around DW center. Once the peak value of ψ comes close to $-\pi$, the order parameters around the peak position relax to another ground state with $\psi = -\pi$. This weakens clamping force between $x_c(\text{Fe})$ and $x_c(\text{P})$ thus ME-DW splits. The same mechanism applies to M-DW and P crossing 0 is the condition in this case.

Two points are important in the splitting process. First, this splitting is a purely dynamical phenomenon, since generating a second DW costs an additional energy due to the gradient terms. Secondly, the inner structure of DW, especially the modulation of originally non-flipping order parameter, plays an important role in the process.

5. Analytical approach for dynamics of ME-DW

In the last part, we use an analytical approach for studying the dynamics of ME-DW. The numerical results in the previous section show that the DW velocity $v(c, H)$ is a smooth function of both c and H near the decoupling limit $c = 0$. We will perform a perturbative expansion for the solution of the TDGL equations and analytically determine the value of v_{21} in Eqs. (15) and (16).

For simplicity, we make an approximation that the antiferromagnetic order parameters N and \mathbf{n} are confined in the xy -plane and they do not change their amplitude

$$\mathbf{N} = N_0(\cos \phi, \sin \phi, 0), \quad \mathbf{n} = n_0(\cos \psi, \sin \psi, 0). \quad (17)$$

This is justified if the anisotropy $\alpha_z - (\alpha_x + \alpha_y)/2$ of Fe spins is large compared with $|c|$. This simplification reduces the number of order parameter fields from seven (N , \mathbf{n} , and P) to three (ϕ , ψ , and P). As in Sec. 3, we study the case that the order parameters varies only along the x -direction. With the approximation above, the free energy density (1b) is rewritten as

$$\begin{aligned} \mathcal{F} = & \frac{\kappa}{2}(\partial_x \phi)^2 - \frac{B}{4} \cos 2\phi - H \cos \phi + \frac{\kappa'}{2}(\partial_x \psi)^2 \\ & + \frac{K}{2}(\partial_x P)^2 + \frac{A}{2}P^2 + c P \cos(\phi - \psi), \end{aligned} \quad (18)$$

where $B \equiv N_0^2(\alpha_y - \alpha_x) > 0$ and a constant is dropped. Here, the parameters are renormalized as:

$$N_0^2 \kappa \rightarrow \kappa, \quad n_0^2 \kappa' \rightarrow \kappa', \quad N_0 H \rightarrow H, \quad N_0 n_0 c \rightarrow c. \quad (19)$$

Let us obtain a stationary state in which a DW travels with

a constant velocity v driven by an external field. To this end, it is convenient to rewrite the TDGL equation in the frame moving together with DW, and define the comoving coordinate $\xi = x - vt$. This comoving frame replaces time and space derivatives as $\partial_t \rightarrow -v\partial_\xi$ and $\partial_x \rightarrow \partial_\xi$, and transforms the TDGL equations into a set of ordinary differential equations (ODE) in ξ . It is important to note that the value of v needs to be determined self-consistently. In this sense, the present task is similar to an eigenvalue problem of quantum mechanics in one dimension.

The stationary TDGL equations thus calculated read as

$$-\frac{v}{\gamma} \dot{\phi}(\xi) = \kappa \ddot{\phi} + \frac{B}{2} \sin 2\phi - H \sin \phi + c P \sin(\phi - \psi), \quad (20a)$$

$$-\frac{v}{\gamma'} \dot{\psi}(\xi) = \kappa' \ddot{\psi} - c P \sin(\phi - \psi), \quad (20b)$$

$$-\frac{v}{\Gamma} \dot{P}(\xi) = K \ddot{P} - AP - c \cos(\phi - \psi), \quad (20c)$$

where a dot symbol denotes the derivative in ξ . Note that the system size is set infinite $-\infty < x < \infty$ in the following analysis.

When $H=0$, uniform stationary states are easily calculated at, and there are four stable solutions corresponding to Eqs. (7): $(\phi, \psi, P) = (0, 0, -c/A)$, $(\pi, \pi, -c/A)$, $(0, \pi, +c/A)$, $(\pi, 0, +c/A)$. Other solutions with $\phi = \pm\pi/2$ are unstable due to their large value of \mathcal{F} .

For a ME-DW solution, we choose the following boundary conditions

$$\begin{aligned} \phi(-\infty) &= 0, \quad \phi(+\infty) = \pi, \quad \psi(\pm\infty) = 0, \\ P(-\infty) &= -c/A, \quad P(+\infty) = +c/A. \end{aligned} \quad (21)$$

For later use, let us examine how the sign change $c \rightarrow -c$ transforms a solution of Eqs. (20). It is easy to check that $(\phi, \psi, -P)$ is a solution for the coupling $-c$ with v unchanged. This means that P is an odd function of c while ϕ , ψ , and v are even. The transformation upon field reverse $H \rightarrow -H$ is more nontrivial, but we have found the necessary transformation

$$\phi(\xi) \rightarrow \pi - \phi(-\xi), \quad \psi(\xi) \rightarrow -\psi(-\xi), \quad P(\xi) \rightarrow -P(-\xi). \quad (22)$$

and this also proves a natural expectation $v(c, -H) = -v(c, H) = -v(-c, H)$.

5.1 Case $c = 0$

Let us summarize the result for a DW solution at $c = 0$, which is a start of perturbation analysis. When $c = 0$, the three order parameters are decoupled in Eq. 20, and only ϕ has a nontrivial solution, which is a DW. This is because spin anisotropy B generates a characteristic length scale $\ell_0 = \sqrt{\kappa/B}$ that determines a DW width. In case of no drive $H = 0$, the stationary velocity is $v = 0$, and Eq. (20a) is reduced to the time-independent sine-Gordon equation $\ddot{\phi} - (2\ell_0^2)^{-1} \sin 2\phi = 0$, and this has a static kink soliton solution $\phi_s(x) = \pi/2 \pm \sin^{-1} \tanh(x/\ell_0)$. This describes a DW connecting two stable states $\phi = 0$ and $\phi = \pi$. Upon applying a driving field H , this DW moves and its motion is described by

an exact solution found by Walker¹⁶⁾

$$\phi_s(\xi) = \frac{\pi}{2} + \sin^{-1}(\tanh q\xi), \quad q \equiv \ell_0^{-1} = \sqrt{\frac{B}{\kappa}}, \quad (23)$$

where the + sign is chosen to satisfy the boundary conditions (21). Here, $\xi = x - v(H)t$ and the velocity is

$$v(H) = \mu_0 H, \quad \mu_0 = 2\gamma \left[\int_{-\infty}^{\infty} d\xi \dot{\phi}(\xi)^2 \right]^{-1} = \frac{\gamma}{q}. \quad (24)$$

Thus, the velocity is linear in H with no higher-order corrections. Its coefficient μ_0 is a mobility of domain wall.

5.2 Effects of $c \neq 0$

Now, let us analyze the effects of the coupling c on the velocity $v(c, H)$ of ME-DW driven by an external field using a perturbation approach. Following a standard procedure, we expand the velocity v and the order parameters in Eqs. (20a)-(20c) in the coupling constant c and driving field H . Recall the parity of the order parameters upon $c \rightarrow -c$, which was discussed before. This restricts the expansion in c as

$$v = \mu_0 H + \sum_{n=1}^{\infty} \sum_{m=0}^{\infty} v_{2n,2m+1} c^{2n} H^{2m+1}, \quad (25a)$$

$$\phi(\xi) = \phi_s(\xi) + \sum_{n=1}^{\infty} \sum_{m=0}^{\infty} \phi_{2n,m}(\xi) c^{2n} H^m, \quad (25b)$$

$$\psi(\xi) = \sum_{n=1}^{\infty} \sum_{m=0}^{\infty} \psi_{2n,m}(\xi) c^{2n} H^m, \quad (25c)$$

$$P(\xi) = \sum_{n=1}^{\infty} \sum_{m=0}^{\infty} P_{2n-1,m}(\xi) c^{2n-1} H^m. \quad (25d)$$

The transformation (22) upon $H \rightarrow -H$ implies that $\phi_{2nm}(\xi)$, $\psi_{2nm}(\xi)$, and $P_{2n+1m}(\xi)$ are an odd function of ξ for even m and an even function for odd m .

The expansion coefficients $v_{2n,2m+1}$, $\phi_{2n,m}$, and others are to be determined successively from lower order to higher order.

In the perturbative approach, we insert the expansions Eq. (25) into Eqs. (20) and compare the terms of the same order $c^n H^m$ on both sides of the equations. Our goal is the first nontrivial correction to the velocity and that is v_{21} . We list up the lowest orders in the expansion up to $O(c^2 H)$, where v_{21} first appears.

$$O(c) : \quad \mathcal{L}_p P_{10} = -K^{-1} \tanh q\xi, \quad (26a)$$

$$O(cH) : \quad \mathcal{L}_p P_{11} = -(\Gamma K)^{-1} \mu_0 \dot{P}_{10}, \quad (26b)$$

$$O(c^2) : \quad \mathcal{L}_q \phi_{20} = -\kappa^{-1} P_{10} \operatorname{sech} q\xi, \quad (26c)$$

$$O(c^2 H) : \quad \mathcal{L}_q \phi_{21} = -\kappa^{-1} (\phi_{20} \tanh q\xi + P_{11} \operatorname{sech} q\xi) - (\gamma \kappa)^{-1} (v_{21} q \operatorname{sech} q\xi + \mu_0 \dot{\phi}_{20}), \quad (26d)$$

where we have used the relations $\cos \phi_s(\xi) = -\tanh q\xi$, and $\sin \phi_s(\xi) = \operatorname{sech} q\xi = q^{-1} \dot{\phi}_s(\xi)$. Here, \mathcal{L}_p and \mathcal{L}_q are differen-

tial operators defined as

$$\mathcal{L}_p \equiv \partial_x^2 - p^2, \quad p \equiv \sqrt{A/K}, \quad (27a)$$

$$\mathcal{L}_q \equiv \partial_x^2 - q^2 \cos 2\phi_s = \partial_x^2 + q^2 (2 \operatorname{sech}^2 q\xi - 1) \quad (27b)$$

We can solve the ODEs (26) by convolution with the Green function of the operators \mathcal{L}_p and \mathcal{L}_q . \mathcal{L}_p is a modified Helmholtz operator, and its Green function G_p is elementary. \mathcal{L}_q is a complicated operator but related to a quantum Hamiltonian for which all the eigenvalues and eigenfunctions are known.^{35,36)} Using these results, we have calculated the corresponding Green function G_q .

$$2p G_p(\xi, \eta) = -e^{-p|\xi-\eta|}, \quad (28a)$$

$$4q G_q(\xi, \eta) = q|\xi - \eta| \operatorname{sech} q\xi \operatorname{sech} q\eta - e^{-q|\xi-\eta|} (1 + \tanh q\xi \tanh q\eta). \quad (28b)$$

Note that these are symmetric: $G_p(\xi, \eta) = G_p(\eta, \xi)$ and $G_q(\xi, \eta) = G_q(\eta, \xi)$.

We can solve equations (26a)-(26c) successively using these Green functions:

$$P_{10}(\xi) = K^{-1} G_p(\xi, \eta) \circ \tanh q\eta, \quad (29a)$$

$$P_{11}(\xi) = (\Gamma K)^{-1} \mu_0 G_p(\xi, \eta) \circ \partial_{\eta} [G_p(\eta, \zeta) \circ \tanh q\zeta], \quad (29b)$$

$$\phi_{20}(\xi) = (\kappa K)^{-1} G_q(\xi, \eta) \circ [\operatorname{sech} q\eta G_p(\eta, \zeta) \circ \tanh q\zeta], \quad (29c)$$

where the circle symbol denotes a convolution $G_r(\xi, \eta) \circ f(\eta) \equiv \int_{-\infty}^{\infty} d\eta G_r(\xi, \eta) f(\eta)$, ($r = p, q$).

We want to obtain v_{21} and it appears in Eq. (26d). However, this equation contains a still unknown function ϕ_{21} . It is possible to obtain v_{21} without calculating this. Notice that the operator \mathcal{L}_q has an eigenfunction with zero eigenvalue:

$$\mathcal{L}_q \Psi_0(\xi) = 0, \Rightarrow \Psi_0(\xi) = \operatorname{sech} q\xi. \quad (30)$$

Take an inner product between Ψ_0 and Eq. (26d), and then the left-hand side vanish because of the self-duality of \mathcal{L}_q . Thus,

$$\begin{aligned} 2v_{21} &= -\mu_0 q (\operatorname{sech} q\xi \tanh q\xi, \phi_{20}) \\ &\quad - \gamma (\operatorname{sech} q\xi, \phi_{20} \tanh q\xi + P_{11} \operatorname{sech} q\xi) \\ &= -\gamma (\operatorname{sech}^2 q\xi, P_{11}) - 2\gamma (\operatorname{sech} q\xi \tanh q\xi, \phi_{20}). \end{aligned} \quad (31)$$

where $(f, g) = \int_{-\infty}^{\infty} d\xi f(\xi) g(\xi)$. We have used a partial integration for the term on the right-hand side in the first line. The value of v_{21} is finally calculated as

$$v_{21} = v_{21}^{(1)} + v_{21}^{(2)}, \quad (32)$$

$$\begin{aligned} v_{21}^{(1)} &= (8p\Gamma K)^{-1} \kappa \mu_0 \int_{-\infty}^{\infty} d\xi \operatorname{sech}^2 q\xi \\ &\quad \times \int_{-\infty}^{\infty} d\eta e^{-p|\xi-\eta|} \int_{-\infty}^{\infty} d\zeta \operatorname{sgn}(\eta - \zeta) e^{-p|\eta-\zeta|} \tanh q\zeta, \end{aligned} \quad (33)$$

$$v_{21}^{(2)} = (p\Gamma K)^{-1} \kappa \mu_0 \int_{-\infty}^{\infty} d\xi \operatorname{sech} q\xi \tanh q\xi$$

$$\times \int_{-\infty}^{\infty} d\eta G_q(\xi, \eta) \operatorname{sech} q\eta \int_{-\infty}^{\infty} d\zeta e^{-p|\eta-\zeta|} \tanh q\zeta. \quad (34)$$

We have performed this numerical integration and

$$v_{21} = -569 \quad (35)$$

This agrees quite well with the fitting result in Sec. 3, $v_{21}^{\text{fit}} = -601$.

In this section, we have shown a perturbative calculation for the stationary dynamics of ME-DW driven by magnetic field. Our calculations justify the perturbative expansion of the terminal velocity $v(c, H)$ in both parameters c and H , and provide a method for systematic improvements by including higher order terms. Expanded functions $\phi_{2n,m}$ and others show how the inner structure of ME-DW deforms in the stationary state from their static solution at $H = 0$, and thus provide important information for understanding the DW dynamics.

6. Conclusion

In this paper, we have studied the dynamics of composite domain walls in a system with three coupled order parameters. The system models the multiferroic material GdFeO_3 , and two antiferromagnetic order parameters of Fe and Gd spins interact with Gd-ion displacement, which leads to electric polarization. The main issue is how the interaction c of the order parameters changes the dynamics of DW. The multiferroic phase has three types of composite DW and we have studied two of them: magneto-electric DW and magnetic DW. We have employed a phenomenological Ginzburg-Landau model for describing this multiferroic system, and calculated how coupling c is related to parameters of the microscopic spin Hamiltonian.

In Sec.3, we have numerically solved the corresponding time-dependent Ginzburg-Landau equations when magnetic field H is applied to drive a DW and calculated the DW velocity v in the stationary state. Analysis with varying H and c shows that the effective DW mobility v/H shows a monotonic decrease with c for both types of DW. This is consistent with an intuitive picture that the interaction c provides a dragging of the order parameter fields not directly coupled to H , and that dissipates a DW motion. It also shows a monotonic increase with H for both DW types but the mobility never exceeds the value μ_0 at $c = 0$, which corresponds to a non-composite DW in Fe antiferromagnetic order. However, its characteristics are quantitatively quite distinct between the two types. The mobility is a smooth function of both H and c for magneto-electric DW, and we have confirmed its analyticity by a perturbation theory in Sec.5 and calculated the leading correction in its c -dependence. This theory provides a formulation for systematic calculation of further higher order terms of not only DW velocity but also deformation in spatial structure of the order parameters. In contrast to this, the mobility of magnetic DW seems to depend on c non-analytically.

This is related to another interesting finding discussed in Sec.4. That is a splitting instability of DW when driving magnetic field exceeds a critical value. A magneto-elastic DW splits into a pair of magnetic DW and elastic DW, while a

magnetic DW splits into a pair including a magneto-elastic DW. One should note that the splitting occurs in bulk without impurity effects. An important difference between the two DW types is that the splitting occurs in the large- c region for magneto-elastic DW but in the small- c region for magnetic DW. There is a narrow reentrant region where a magneto-elastic DW becomes unstable for intermediate H but stabilized again at very large H . Thus, magnetic DW is more singular than magneto-elastic DW regarding its nonanalytic c -dependence of the mobility and quick instability with H . This is due to that fact that an evolution of magnetic DW upon switching c is not analytic in the part of Gd antiferromagnetic order parameter. It is characterized by a divergent length scale originating in the spin rotation symmetry at $c = 0$, and a finite length scale generated by the coupling to Fe order parameter has a singular behavior in c . To describe these non-analytic characteristics qualitatively, we need further analyses but leave them for a future study.

- 1) N.A. Spaldin and M. Fiebig, *Science* **309**, 391 (2005).
- 2) D.I. Khomskii, *J. Mag. Mag. Mat.* **306**, 1 (2006).
- 3) S.-W. Cheong and M. Mostovoy, *Nat. Mat.* **6**, 13 (2007).
- 4) Y. Tokura and S. Seki, *Adv. Mat.* **22**, 1554 (2010).
- 5) Y. Tokura, S. Seki, and N. Nagaosa, *Rep. Prog. Phys.* **77**, 076501 (2014).
- 6) J.M. Perez-Mato, S.V. Gallego, L. Elcoro, E. Tasci, and M.I. Aroyo, *J. Phys. Cond. Matt.* **28**, 286001 (2016).
- 7) See for a review, N.D. Mermin, *Rev. Mod. Phys.* **51**, 591 (1979).
- 8) Y. Tokunaga, N. Furukawa, H. Sakai, Y. Taguchi, T. Arima, and Y. Tokura, *Nat. Mater.* **8**, 558 (2009).
- 9) T. Kimura, T. Goto, H. Shintani, K. Ishizaka, T. Arima, and Y. Tokura, *Nature (London)* **426**, 55 (2003).
- 10) T. Choi, Y. Horibe, H.T. Yi, Y.J. Choi, W. Wu, and S.W. Cheong, *Nat. Mater.* **9**, 253 (2010).
- 11) S. Ishiwata, Y. Kaneko, Y. Tokunaga, Y. Taguchi, T. Arima, and Y. Tokura, *Phys. Rev. B* **81**, 100411 (2010).
- 12) M. Bibes and A. Barthélémy, *Nat. Mater.* **7**, 425 (2008).
- 13) K.D. Belashchenko, O. Tchernyshov, A.A. Kovalev, and O.A. Tretiakov, *Appl. Phys. Lett.* **108**, 132403 (2016).
- 14) F. Kagawa, M. Mochizuki, Y. Onose, H. Murakawa, Y. Kaneko, N. Furukawa, and Y. Tokura, *Phys. Rev. Lett.* **102**, 057604 (2009).
- 15) Y. Tokunaga, Y. Taguchi, T. Arima, and Y. Tokura, *Nat. Phys.* **8**, 838 (2012).
- 16) N.L. Schryer and L.R. Walker, *J. Appl. Phys.* **45**, 5406 (1974).
- 17) G.S.D. Beach, C. Nistor, C. Knutson, M. Tsoi, and J.L. Erskine, *Nat. Mater.* **4**, 741 (2005).
- 18) L. Berger, *Phys. Lett. A* **46**, 3 (1973).
- 19) G. Tatara, H. Kohno, and J. Shibata, *Phys. Rep.* **468**, 213 (2008).
- 20) X.H. Zhu, X.B. Xiao, X.R. Chen, and B.G. Liu, *RSC Advances* **7**, 4054 (2017).
- 21) M. Matsubara, S. Manz, M. Mochizuki, T. Kubacka, A. Iyama, N. Aliouane, T. Kimura, S.L. Johnson, D. Meier, and M. Fiebig, *Science* **348**, 1112 (2015).
- 22) M. Darakchiev, G. Catalan, and J.F. Scott, *Phys. Rev. B* **81**, 224118, (2010).
- 23) E.A. Eliseev, A.N. Morozovska, C.T. Nelson, and S.V. Kalinin, *Phys. Rev. B* **99**, 014112 (2019).
- 24) I. Dzyaloshinsky, *J. Phys. Chem. Sol.* **4**, 241 (1958).
- 25) T. Moriya, *Phys. Rev.* **120**, 91 (1960).
- 26) S. Geller, *J. Chem. Phys.* **24**, 1236 (1956).
- 27) A.A. Mukhin, M. Biberacher, A. Pimenov, and A. Loidl, *J. Mag. Resonance* **170**, 8 (2004).

- 28) M. Das, S. Roy, and P. Mandal, Phys. Rev. B **96**, 174405 (2017).
- 29) E. Bertaut, J. de Phys. Colloques **32**, 462 (1971).
- 30) J.D. Cashion, A.H. Cooke, D.M. Martin, and M.R. Wells, J. Appl. Phys. **41**, 1193 (1970).
- 31) E. Fehlberg, *NASA Technical Report*, NASA TR R-315 (NASA, 1969).
- 32) See for example, J.D. Gunton, M.S. Miguel, and P.S. Sahni in *Phase Transitions and Critical Phenomena*, Vol. 8, (Academic Press, New York, 1983).
- 33) See for example, C. Kittel, Rev. Mod. Phys. **21**, 541 (1949).
- 34) A. Schilling, T.B. Adams, R.M. Bowman, J.M. Gregg, G. Catalan, and J.F. Scott, Phys. Rev. B **74**, 024115 (2006).
- 35) L.D. Landau and E.M. Lifshitz, *Quantum Mechanics*, Third Edition, Sec. 23, (Butterworth Heinemann, London, 2003).
- 36) J. Lekner, Am. J. Phys. **75**, 1151 (2007).